Systematic Analysis of Mass yield Curves in Low-Energy Fission of Actinides

Systematic analysis of mass yield curves in low-energy fission of actinides

T. Ohtsuki, Y. Hamajima, K. Sueki, and H. Nakahara
Tokyo Metropolitan University, Department of Chemistry, Faculty of Science, Fukasawa, Setagaya, Tokyo 158, Japan

Y. Nagame, N. Shinohara, and H. Ikezoe
Japan Atomic Energy Research Institute, Tokai, Ibaraki 319-11, Japan
(Received 22 May 1989)

Mass yield curves in low-energy proton-induced fissions of ^{233}U, ^{235}U, ^{238}U, ^{237}Np, ^{239}Pu, ^{242}Pu, ^{244}Pu, ^{241}Am, and ^{243}Am were measured. The full widths at half maximum (FWHM) of the heavier asymmetric peak of the mass yield curves showed a sudden dip in the region of $A_f = 240-245$. The correlation between the P/V ratio and the FWHM of the asymmetric mass yield peak was obtained as a function of proton energy. The FWHM values were independent of the incident proton energy as long as the P/V ratio was larger than 10 for all the fissioning systems studied. The excitation energy dependence of the mass yield curves was investigated. It was found that the excitation energy dependence of symmetrically divided fission products was apparently different from that of asymmetrically divided ones. With a simple assumption of the two-mode hypothesis, the observed mass yield curves could be decomposed into two mass yield curves. Asymmetric mass yield peaks could be best represented by the sum of two Gaussians, and their variation could be expressed by the variation of Gaussian parameters. The peak positions of the two Gaussians were always $A = 133-135$ and $A = 140-142$ for all the investigated fissioning nuclides. The preference of those fragment masses is discussed in terms of both the scission-point model and the saddle-point model.

I. INTRODUCTION

The correlation of the mass asymmetry in fission with nuclear shell structure was first pointed out by Goeppert-Mayer in 1948.[1] But due to a lack of a proper model which could describe the shell effect at moderate and large deformations, it was only in 1970 that the effect of nuclear shell structure on the stabilization of the reflection asymmetric saddle was theoretically demonstrated by Möller *et al.*[2,3] by using the Strutinsky prescription.[4] A strong correlation was then shown by Ledergerber and Pauli[5] between the experimental peak-to-peak mass ratio of the asymmetric mass distribution and the mass ratio of the two halves of the nucleus at the outer saddle. Such a correlation supports a speculation that nucleons "feel" the shell structure of the future fragments already at unconstricted but sufficiently stretched shapes, and that they conserve their composition all the way down to scission. On the other hand, Wilkins *et al.*[6] applied the Strutinsky shell correction method to the two deformed nuclei in contact at scission and calculated mass, charge, and kinetic energy distributions with an assumption of a quasi-equilibrium among collective degrees of freedom. Their calculations can explain the general trend of the distributions of nuclear mass, nuclear charge, and kinetic energy in the fission of a wide range of nuclides from Po to Fm isotopes[7–12] although, quantitatively, they can only reproduce much narrower, and somewhat deviated mass yield peaks than the observed ones. However, essential questions remain to be answered on the validity of assuming a well-defined scission configuration. In order to understand the mass division mechanism, more systematic experiments and careful examination of the existing data are needed.

The aim of the present work is to examine the mass division phenomena by studying low-energy proton-induced fissions of actinides. We have observed mass yield curves for the targets of ^{232}Th, ^{233}U, ^{235}U, ^{238}U, ^{237}Np, ^{239}Pu, ^{242}Pu, ^{244}Pu, ^{241}Am, and ^{243}Am. Detailed results will be published elsewhere.[13,14] The observed data are discussed in terms of the systematic variation, as a function of the mass of the fissioning nuclide, of the full width at half maximum of the asymmetric mass yield peak, and the incident energy dependence of the symmetric and asymmetric product yields. The shape of asymmetric mass yield peaks were parametrized by two Gaussians. Finally the influence of the nuclear structures of the fissioning nuclides and fragments on the observed asymmetric mass yield peaks is examined.

EXPERIMENTAL PROCEDURE

The isotopic compositions of the enriched isotopes ^{232}Th, ^{233}U, ^{235}U, ^{238}U, ^{237}Np, ^{239}Pu, ^{242}Pu, ^{244}Pu, ^{241}Am, and ^{243}Am used as targets were over 99%. They were chemically purified and electrodeposited on a 6 mg/cm^2 Al foil. The thickness of each target was determined by α spectrometry to be 100–300 μg/cm^2. Each target foil was wrapped with a sheet of Al foil (6 mg/cm^2), which was thick enough to stop all fission products. Six to eight wrapped targets were stacked for proton bombardments. 10 mg/cm^2 Cu foils were inserted into the target stack at an appropriate interval for beam current monitoring.

Bombardments were performed at the Japan Atomic Energy Research Institute (JAERI) tandem accelerator and at the AVF cyclotron of Institute for Nuclear Study

TABLE I. Reactions of proton-induced fissions and the range of the incident energy.

Reaction	E_p (MeV)
^{232}Th+p[a]	8–22
^{233}U+p	9–16
^{235}U+p	12,18
^{237}Np+p	9–32
^{238}U+p	10–24
^{239}Pu+p	9–16
^{241}Am+p	12–15
^{242}Pu+p	12,18
^{243}Am+p	12,18
^{244}Pu+p	12,18

[a]From Ref. 28.

(INS) with the beam current of about 1 μA. The proton energies on the target are listed in Table I.

After the bombardment, γ-ray activities produced in each target-catcher assembly were measured directly with a Ge(Li) detector equipped with a 4098 channel pulse-height analyzer.[15] The produced nuclides were identified from their characteristic γ-ray energies, and their formation cross sections were evaluated from the observed photopeak areas and from the beam current determined by the Cu monitor. The reaction cross-section data reported by Collé *et al.*[16] for protons on Cu were used. The incident proton energy on each target was estimated from the range-energy relations reported by Williamson *et al.*[17] and Northcliffe and Schilling.[18]

RESULTS

Mass yield curves were constructed from the observed cross section of each fission product to which a correction was applied,when necessary, for the charge distribution by assuming a Gaussian charge distribution with the most probable charge Z_p of unchanged-charge division. The Gaussian width parameter of 0.95 was used as suggested by J. A. McHugh *et al.*[19] The correction was large for ^{127}Sb, ^{129}Sb, ^{132}Te, and ^{135}Xe. The mass yield curves thus obtained for the fissions at $E_p = 12$ MeV are shown in Fig. 1. The uncertainty of each data point is not shown in the figure, but it is typically about 10%.

All the mass yield curves are asymmetric as expected, but the width of the asymmetric peak and the depth of the symmetric valley are different. It is interesting to note that even though the mass number is different by only one unit between the compound nuclei formed by (^{232}Th+p) and (^{233}U+p) reactions, the mass yield curve of the former fission has a much broader valley in the symmetric region than that of the latter. The valley width, in general, becomes narrower as the fissioning

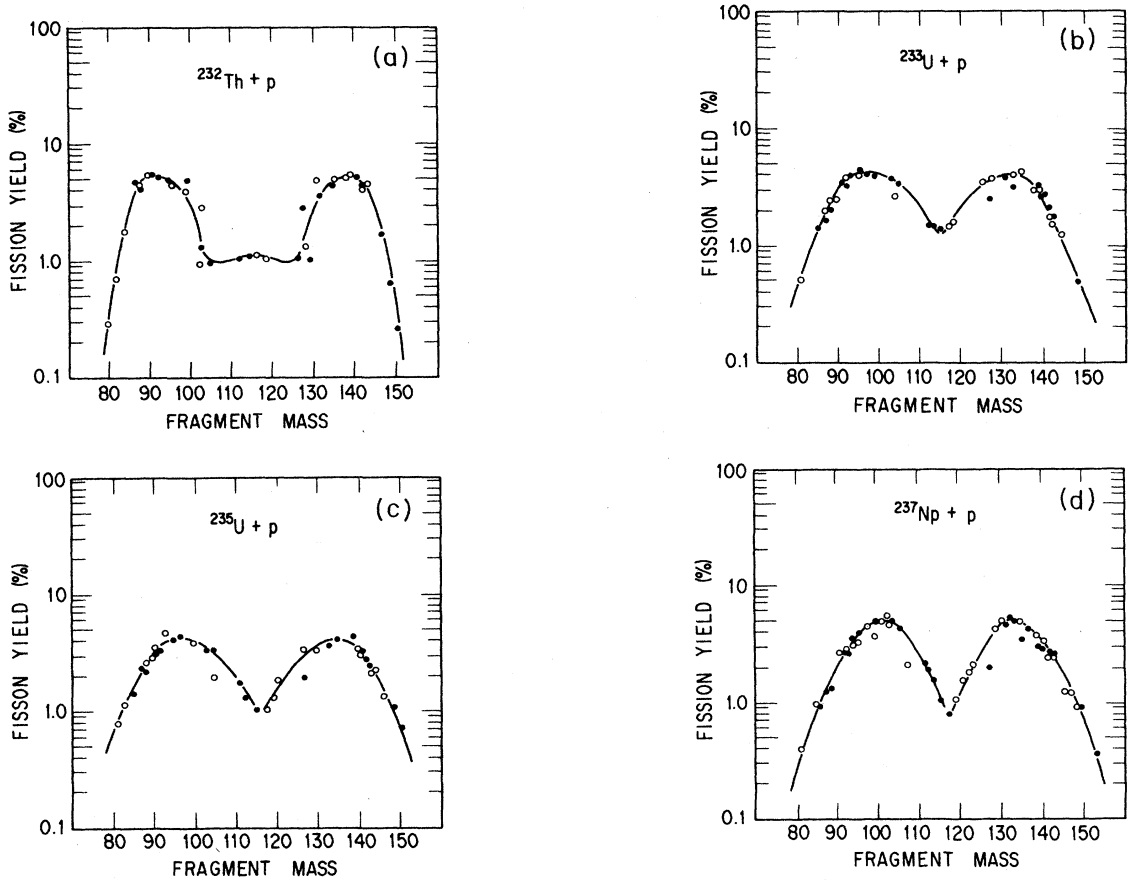

FIG. 1. Mass yield curves of the proton-induced fission of ^{232}Th (from Ref. 28), ^{233}U, ^{235}U, ^{237}Np, ^{238}U, ^{239}Pu, ^{241}Am, ^{242}Pu, ^{243}Am, and ^{244}Pu. Solid circles indicate the observed chain yields and open circles are their reflected points.

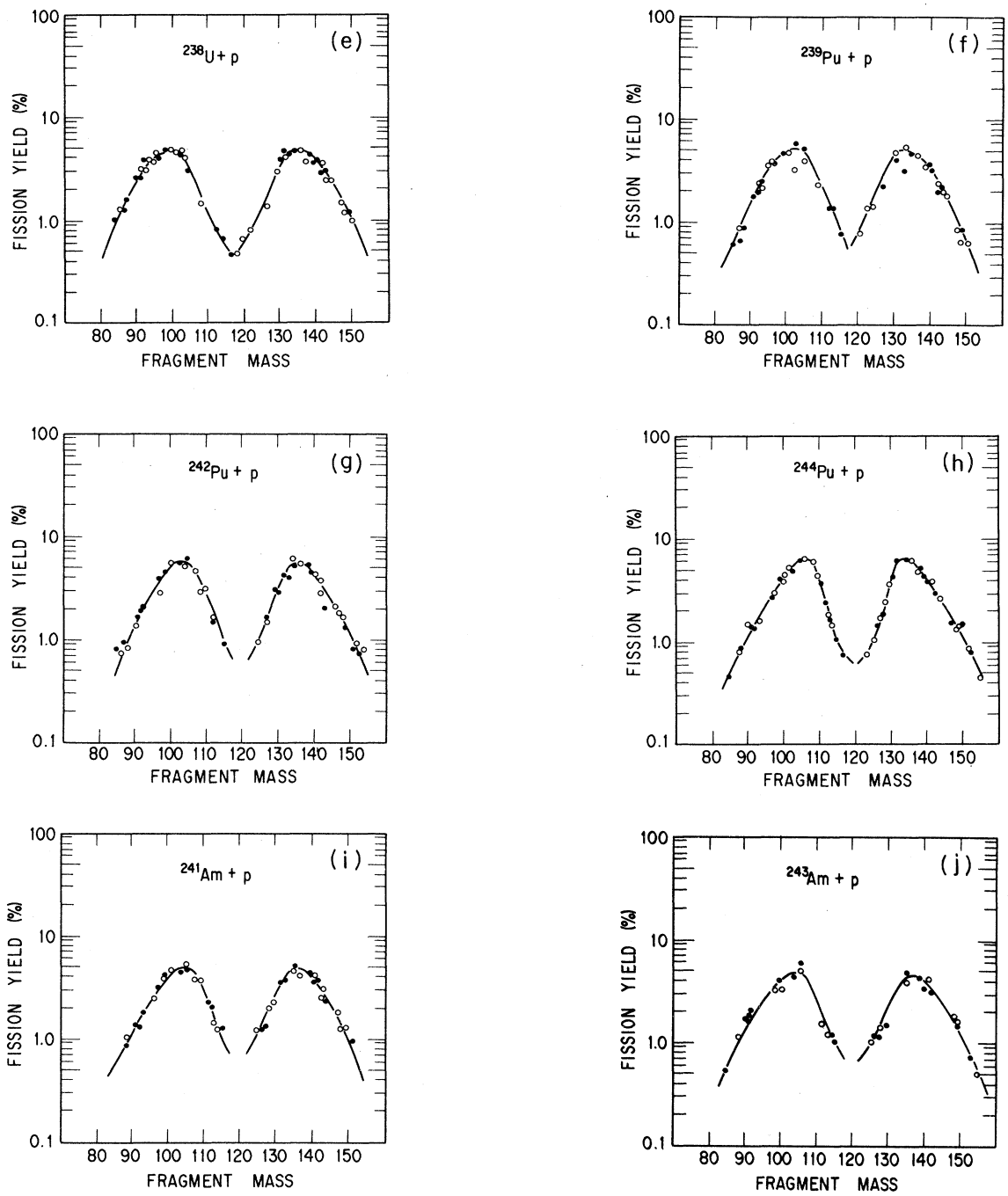

FIG. 1. (*Continued*).

mass A_f becomes larger. The weighted mean mass of the heavier asymmetric peak varies only slightly over the broad mass range of the compound nucleus A_f as shown in Fig. 2. (As the mean mass of the actual fissioning nuclides cannot be determined experimentally in the present study, the mass of the compound nucleus is often shown as A_f. They are different by no more than two mass units in the proton energy range of the present work.) This observation is in agreement with the well-known trend reported for thermal-neutron–induced fissions and spontaneous fissions,[7,20–24] although the mass interval between the mean of the lighter asymmetric peak and that of the heavier one is somewhat narrower in proton-induced fissions.

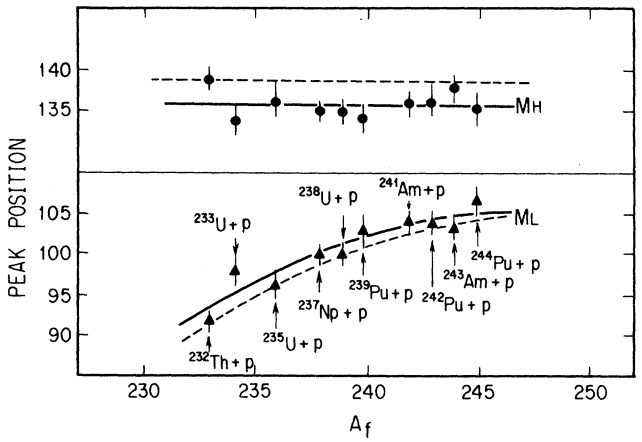

FIG. 2. Weighted mean peak positions of light and heavy asymmetric peaks in the fissions of various nuclides. Closed solid circles are the peak positions of the heavy asymmetric peaks, and solid triangles are those of the light asymmetric peaks. Solid lines are drawn through the data points to guide eyes. Dashed lines are for thermal-neutron induced fissions.

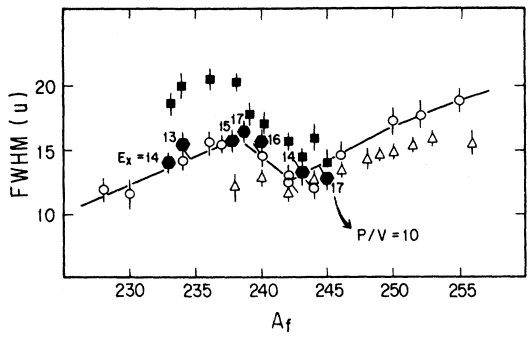

FIG. 3. Full width at half maximum (FWHM) values as a function of fissioning mass. Closed squares are the FWHM values of proton-induced fissions observed in this work. Open circles are those of thermal-neutron–induced fissions; open triangles, those of spontaneous fissions; and solid hexagonal symbols, those of proton-induced fissions that give $P/V=10$. E_x is the excitation energy of the compound nucleus that gives rise to the mass yield curve of $P/V=10$.

DISCUSSIONS

A. FWHM of the asymmetric mass yield peak

As reported in Ref. 25, the full width at half maximum (FWHM) of the asymmetric peak becomes minimum at around $A_f=242$ for both thermal-neutron induced and spontaneous fissions (see open symbols in Fig. 3), while that at one-tenth of maximum (FWTM) increases monotonously as A_f increases.[20,26,27] The mass yield data used in the analysis are only those determined radiochemically and not corrected for the effect of post-fission neutron emissions. The decreasing trend in FWHM at $A_f=240-245$ is hardly understood by the liquid drop model, which predicts a smooth increasing trend as a function of the fissioning mass. It reveals the importance of the shell effects of either the fissioning nuclide or the final fragments, or both on the asymmetric mass division.

For further investigation of this trend in FWHM, we examined the mass yield curves observed in this work for 12 MeV proton-induced fissions and showed the results in Fig. 3 with solid squares. The error bar attached to each symbol was estimated from the uncertainty of the yield data. The FWHM values for proton-induced fissions of $A_f=233-238$ are much larger than those for thermal-neutron–induced fissions and the dip around $A_f=240-245$ seems to be more pronounced. For a better understanding of the data, the relation of FWHM with the peak to valley ratio (P/V) observed in proton induced fissions is plotted in Fig. 4. The figure shows that the FWHM decreases as the P/V increases and it approaches the value for thermal-neutron–induced fissions as the P/V ratio becomes larger than about 10 for most of the fissioning systems studied. With a closer examination of the observed mass yield curves, it is found that the increase of the FWHM is mostly caused by the increased yields at the lighter side of the heavier asymmetric peak (the inner side of the peak). This observation leads to a conjecture that the larger FWHM was mostly caused by the larger contribution of the symmetric fission. As the effect of the symmetric valley region on the width of the asymmetric peak becomes small at around $P/V=10$, the FWHM values at $P/V=10$ estimated from Fig. 4 are plotted in Fig. 3 by hexagonal symbols. The excitation energy of the compound nucleus with which the P/V ratio becomes 10 differs in this kind of plot by as much as 4 MeV as shown by Arabic numerals. Among seven hexagonal symbols, the two in the $A_f=240-245$ region have the smallest FWHM, and the dip also appears for the proton induced fission.

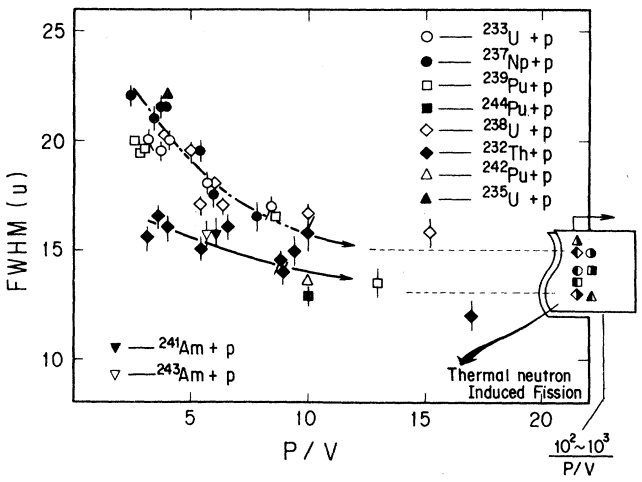

FIG. 4. A relation between the FWHM value and the peak-to-valley ratio (P/V). Symbols used for thermal-neutron induced fissions are ●, ^{233}U+n; ◑, ^{239}Pu+n; ◧, ^{241}Pu+n; ◨, ^{241}Am+n; ◆, ^{236}Np+n; ◆, ^{229}Th+n; ▲, ^{243}Am+n; ▲, ^{235}U+n.

B. Two-mode analysis of mass yield curves

The energy dependence of mass yield curves has been investigated in terms of cross section ratios of each product[28] or peak-to-valley ratios.[29–33] Typical examples of the cross section ratios of several fission products to ^{97}Nb observed in this work are shown as a function of the incident proton energy for the ^{237}Np+p reaction in Fig. 5. The yield ratios of typical asymmetric mass division products themselves, such as ^{105}Rh/^{97}Nb, ^{143}Ce/^{97}Nb, and symmetric mass division products themselves are both independent of the incident proton energy, while the yield ratios of asymmetric to symmetric products such as ^{115}Cd/^{97}Nb are strongly dependent on the incident energy. Similar incident energy dependences of yield ratios were observed in all other fission reactions studied in this

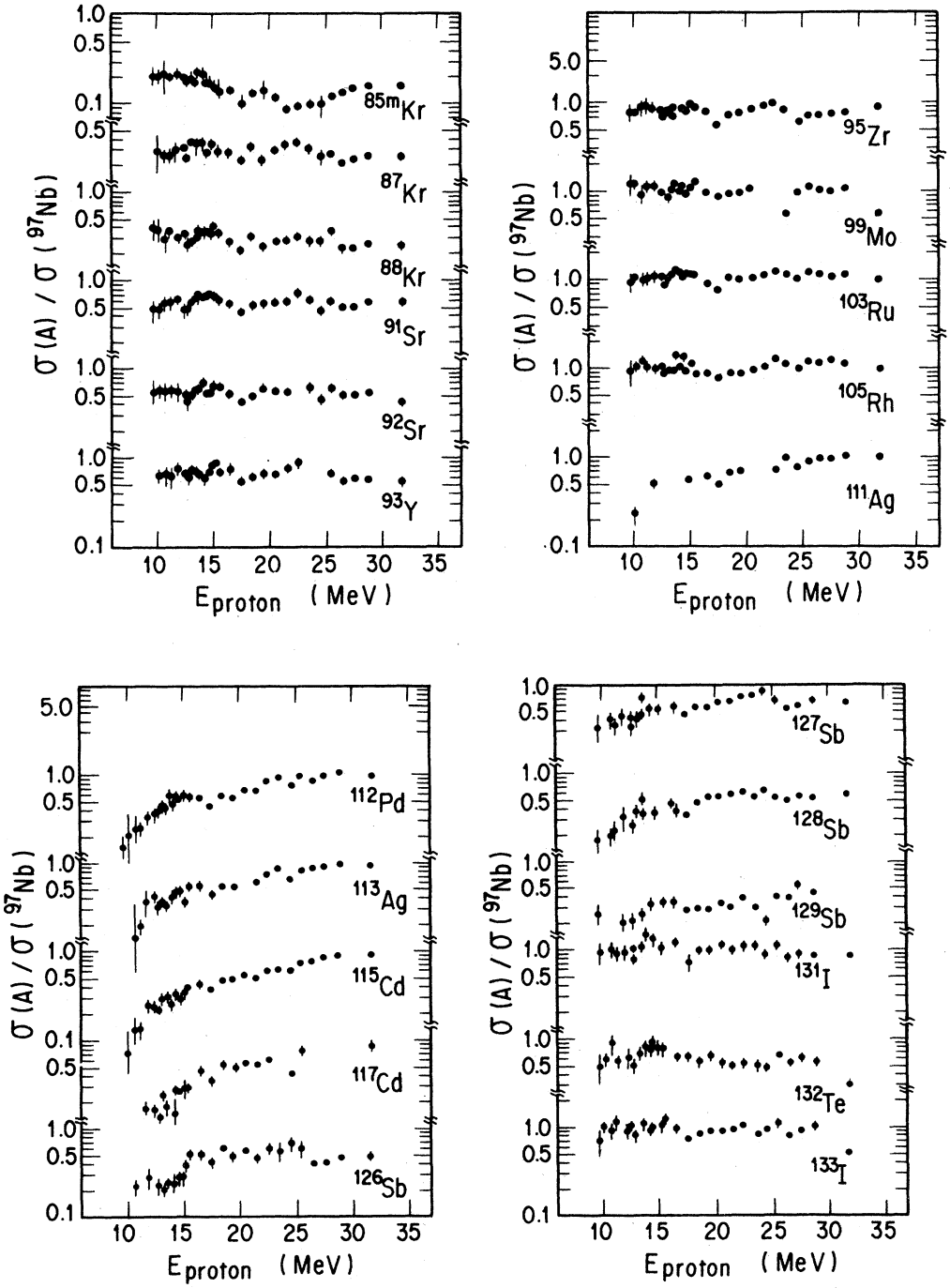

FIG. 5. Cross section ratios $\sigma(A)/\sigma$ (^{97}Nb) as a function of the incident proton energy for the ^{237}Np+p fission.

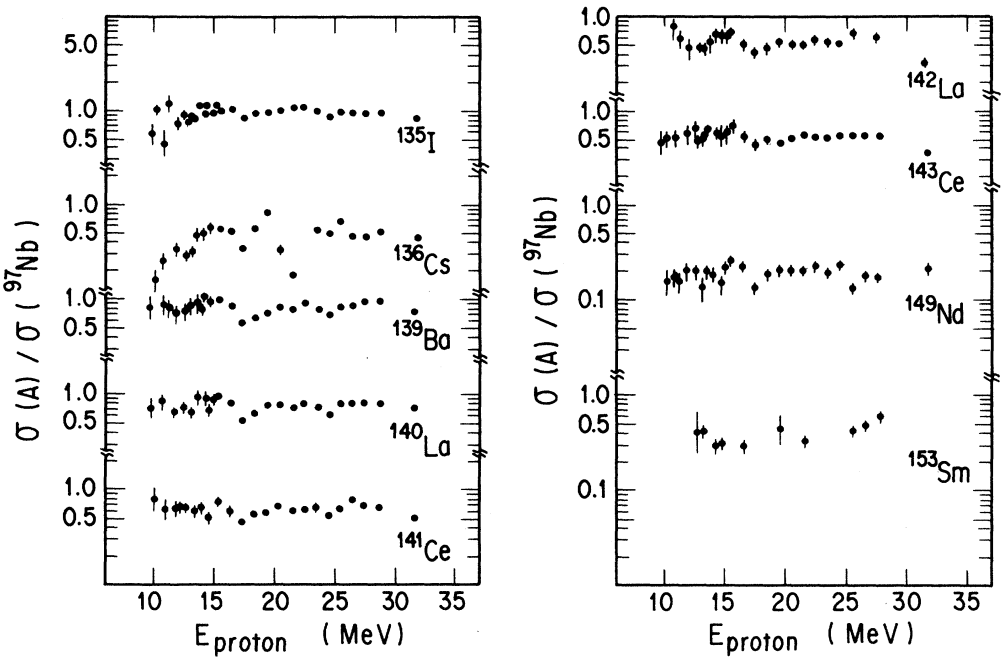

FIG. 5. (*Continued*).

work. Such a distinctively different energy dependence for the symmetric mass division and for the asymmetric mass division suggests as a first approximation the existence of two fission barriers leading to the hypothesis of "two independent modes"[34] first proposed by Turkevich and Niday.[34] The existence of the symmetric and the asymmetric barriers was experimentally deduced by many workers such as Britt *et al.*,[35] Konecny *et al.*,[36] Kudo *et al.*,[28,37] and others.[38–40] Until now, no theory has predicted for the fission of light actinides and the existence of two static saddles, except that claimed by Pashkevich[41] and Brosa *et al.*[42,43] But, as Pauli and Ledergerber[44] have demonstrated, there can be dynamic fission barriers along the paths of deformation which are not necessarily related with static barriers. If two different barriers exist corresponding to the symmetric and asymmetric fission, the phenomena of the increase of the FWHM value as the P/V ratio decreases can be explained by the larger contribution of the symmetric component to the inner side of the asymmetric heavy peak. Another observation mentioned above—namely, that the mass difference between the weighted mean masses of the heavier and the lighter asymmetric peak is smaller for proton-induced fissions than for thermal-neutron–induced fissions and spontaneous fissions—may also be related with the increased symmetric component as the excitation energy of the fissioning nuclide is increased. In the following, an attempt has been made to analyze the observed mass yield curves into the symmetric and asymmetric component with an assumption of two independent fission barriers. The ratio of the observed yield for the fragment mass A to that for A_0 can be described by the following equation:

$$\frac{Y(A,E)}{Y(A_0,E)}=\frac{\sigma_S(E)y_s(A)+\sigma_a(E)y_a(A)}{\sigma_s(E)y_s(A_0)+\sigma_a(E)y_a(A_0)}\ , \tag{1}$$

where $\sigma(E)$ is the cross section of either symmetric or asymmetric fission at the proton energy E, and $y(A)$ is the fractional yield of the fragment mass A in each fission mode. The subscript "a" denotes asymmetric fission and "s" denotes symmetric fission. If $A_0=143$ is taken as a reference mass number, $y_s(A_0)$ may be assumed negligible compared to $y_a(A_0)$. Then, the equation is reduced to a simple linear equation,

$$\frac{Y(A,E)}{Y(143,E)}=\frac{\sigma_s(E)}{\sigma_a(E)}\frac{y_s(A)}{y_a(143)}+\frac{y_a(A)}{y_a(143)}\ . \tag{2}$$

Similarly, if $y_a(115)$ is negligible compared to $y_s(115)$, $\sigma_s(E)/\sigma_a(E)$ can be expressed in terms of $Y(115,E)/Y(143,E)$, and finally,

$$\frac{Y(A,E)}{Y(143,E)}=\frac{Y(115,E)}{Y(143,E)}\frac{y_s(A)}{y_s(115)}+\frac{y_a(A)}{y_a(143)}\ . \tag{3}$$

By plotting the observed $Y(A,E)/Y(143,E)$ against $Y(115,E)/Y(143,E)$ or the V/P ratio, fractional yield ratios within each mode of $y_s(A)/y_s(115)$ and $y_a(A)/y_a(143)$ can be obtained from the slope and the intersection with the ordinate, respectively. In Eq. (1), the fractional yield of a fragment mass A in each fission mode is assumed to be a function of A alone, and not of the incident energy. This assumption is valid if the shape of the mass distribution in each mode does not vary appreciably within the range of the excitation energy investigated in the present work. However, it is known that a

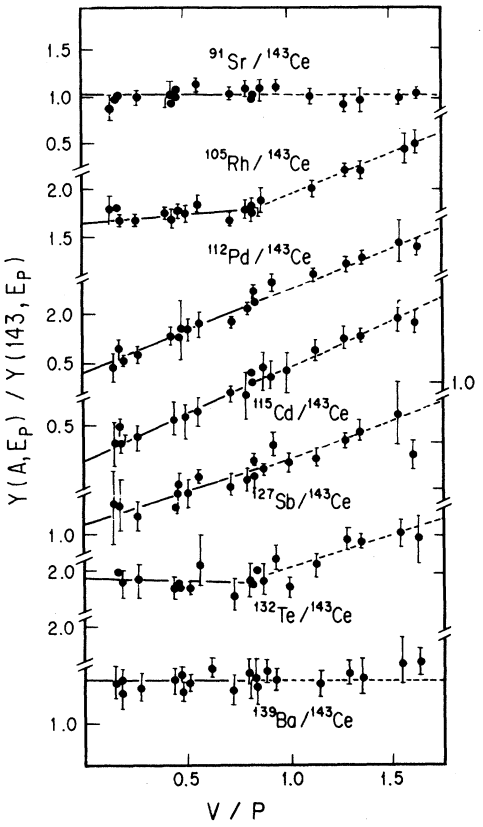

FIG. 6. $Y(A,E_p)/Y(143,E_p)$ ratios as a function of the valley-to-peak ratio. Solid and dashed lines are the results of least-squares fittings.

new channel opens; specifically, another multiple chance fission becomes possible at the proton energy of $\sim$14 MeV.[28] If the effect of the change of the fissioning mass is large on $y(A)$, the linear relationship of Eq. (3) between $Y(A,E)/Y(143,E)$ and $Y(115,E)/Y(143,E)$ will not hold. Such a plot for the observed data in the reaction of (^{237}N+p) is given in Fig. 6. Lines represent least-squares fittings of the data points. Solid and dashed lines indicate that the fissioning nuclide could be different in those two energy regions, especially for the asymmetric mode. Figure 6 shows that a linear relation holds for most of the fragments except for ^{105}Rh and ^{132}Te, which are clearly affected by the onset of a new channel. Then, an analysis was performed only within the energy region shown by solid lines, and the values of $y_s(A)/y_s(115)$ and $y_a(A)/y_a(143)$ were evaluated from the slope and the interception. Such an analysis allows a decomposition of the observed mass yield curve into two components of different threshold energies as shown in Fig. 7 for the 12 MeV proton-induced fission of ^{237}Np. The FWHM values of the extracted asymmetric peaks depicted by the dashed curve in Fig. 7 for ^{237}Np are in good agreement with those for thermal-neutron–induced fissions as shown in Fig. 3. The mass yield curve of the symmetric component is somewhat flat at the top.

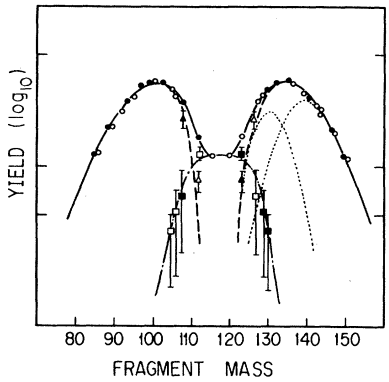

FIG. 7. Mass distribution of the ^{237}Np+p fission at $E_p=12$ MeV. The solid line shows cumulative yields. The dash-dotted lines are the symmetric component, and the broken lines are the asymmetric one obtained by the analysis of Eq. (1). Dotted lines are the result of the two Gaussian fittings to the asymmetric component by Eq. (4).

C. Parametrization of mass yield curve

In order to see the systematic variation of mass yield curves as a function of Z and A of the fissioning nuclide, it would be most appropriate if they can be fitted by some functional forms and understood by the parameters involved. After having tried various functional forms, we have come to a conclusion that a two-Gaussian analysis gives the best fit to all the asymmetric mass yield peaks reported in literature for both spontaneous and thermal-neutron–induced fissions. In the analysis, the fragment mass yield $Y(A)$ is expressed by six parameters X_i, A_i, and σ_i ($i=1,2$) as follows:

$$Y(A)=\sum_{i=1}^{2}\{X_i\exp[-(A-A_i)^2/2\sigma i^2]\}\ , \tag{4}$$

where A_i and σ_i are the peak mass number and the width of the Gaussian, respectively. Some results of such a two-Gaussian analysis for thermal neutron fissions are shown in Fig. 8, and the parameters A_i and σ_i for heavy asymmetric peaks are plotted in Fig. 9 as a function of the mass of the fissioning nuclide A_f. (Circular symbols represent thermal-neutron–induced fissions and triangles represent spontaneous fissions.) Characteristic trends of the parameters extracted from the two-Gaussian analysis are (1) the two peak positions are invariant for all A_f and center around $A=133-135$ and $A=140-142$; (2) the width (σ) of the lighter Gaussian is about 2.5 and stays constant for all A_f, while that of the heavier Gaussian slightly increases in the region of $A_f=230-240$. Recently, Straede *et al.*[47] showed that the mass distribution of the 6 MeV neutron-induced fission of ^{235}U could be decomposed into five Gaussians. Our analysis for thermal-neutron–induced fission around $A_f=235$ is in agreement with their Gaussian width (σ) and the peak position.

We have applied the same two-Gaussian parametrization to the asymmetric mass yield peaks obtained by the

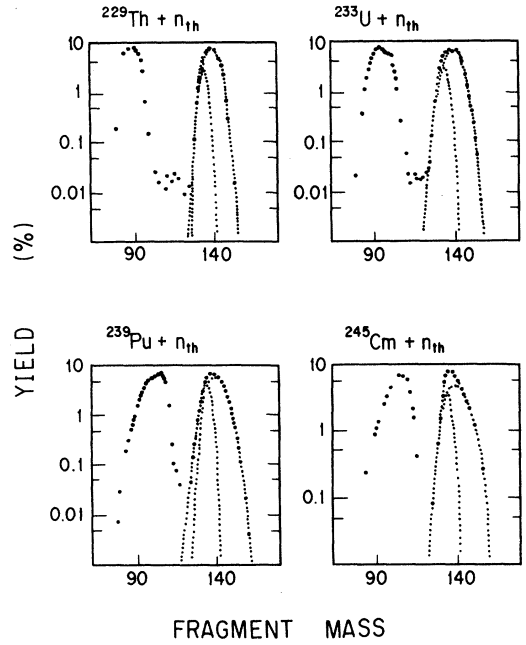

FIG. 8. Two-Gaussian fitting of the heavy asymmetric mass yield peak of thermal-neutron–induced fission. Dotted lines are the results of fitting. The data for ^{229}Th+n, ^{233}U+n, and ^{239}Pu+n are taken from Ref. 45, and those for ^{245}Cm+n from Ref. 46.

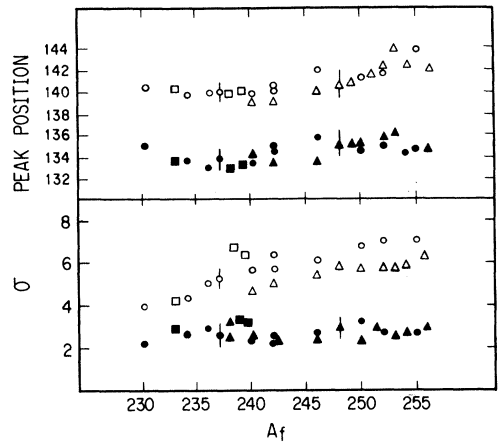

FIG. 9. Parameters obtained by a two-Gaussian fit to the heavy asymmetric peak of the mass distribution versus the mass number of the fissioning nucleus (A_f): the widths, σ, and the peak positions of the heavier (open symbols) and lighter (closed symbols) Gaussians. ■, □ show the results of the two Gaussian fittings to the heavy asymmetric peak obtained by the two-mode analysis for proton induced fissions; ▲, △ for spontaneous fission; ●, ○ for thermal-neutron–induced fission.

two-mode analysis described earlier. The result for (^{237}Np+12 MeV proton) is shown by dotted curves in Fig. 7. The analysis has also been applied to other reactions, ^{232}Th+p and ^{238}U+p, and the parameters are shown in Fig. 9 by square symbols. Another Gaussian parameter determined is the height parameter X_i. Ratios of the heights of the two-Gaussians for the heavy asymmetric peak are plotted in Fig. 10. The ratio of the heavier Gaussian (centering around $A=141$) to the lighter Gaussian (centering around $A=134$) decreases from $A_f=230$ to the minimum at $A_f=242$ and increases again for the larger A_f up to ^{256}Fm. The ratios for thermal-neutron–induced fissions of ^{253}Es and ^{255}Es seem to deviate from this systematic trend, possibly due to the small P/V ratio of the mass yield curve. But those for the asymmetric mode of proton-induced fissions shown by square symbols in the figure follow the systematic trend. The error bars shown in the figure are the curve-fitting errors.

Through the two-Gaussian parametrization, it is found that the FWHM minimum for $A_f=240$–245 shown in Fig. 3 is associated with the minimum ratio of the two Gaussian heights in Fig. 10. At the fissioning mass of $A_f=240$–245, the mass yields around $A=133$–135 (where a narrow Gaussian peaks) become larger relative to those around $A=140$–142, giving rise to a smaller FWHM of the overall mass yield curve.

The constancy of the peak positions and only slight variation of the widths in the two Gaussian analysis of the heavy asymmetric mass yield peak may tempt one to conclude that the fragment shell structure determines the final mass division. The peak position around $A=133$–135 corresponds to the spherical neutron shell at $N=82$, and the constancy of the peak position and the width throughout a wide range of A_f reveals the importance of this fragment shell as pointed out by many previous investigators. The peak position at $A=140$–142 corresponds to the fragments with the neutron number $N=88$, which is predicted by Wilkins *et al.*[6] to cause an extremely deformed stability. The dependence of the relative height of the two Gaussians on A_f, X_2/X_1, cannot be explained, however, by the scission-point model of Wilkins *et al.*[6] In Fig. 11, the difference in the

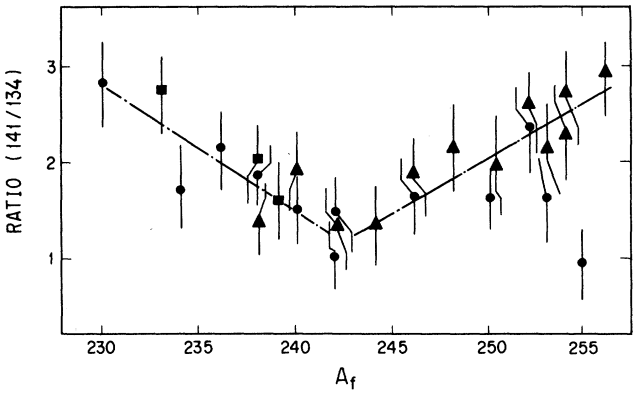

FIG. 10. Peak height ratios of the heavier ($A=140$–142) to the lighter ($A=133$–135) Gaussian as a function of fissioning mass ■ for the proton-induced fission obtained after the two-mode analysis in this work; ♦ for thermal-neutron–induced fission; ▲ for spontaneous fission.

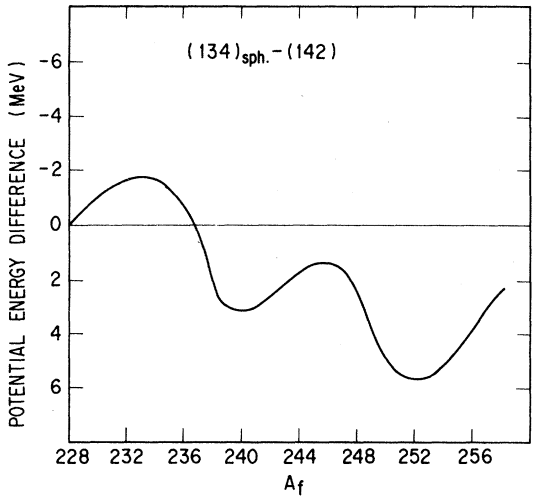

FIG. 11. Difference in the potential minima associated with two particular mass splits (134+complement) and (142+complement) calculated for two touching spheroids by Wilkins *et al.* (Ref. 6).

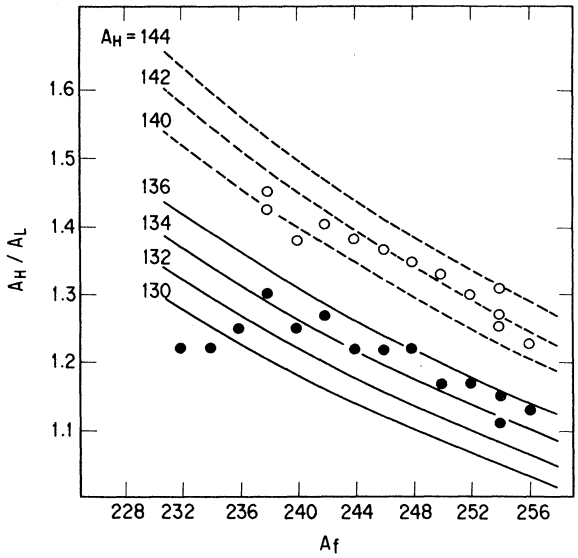

FIG. 12. Heavy-to-light fragment ratios A_H/A_L predicted by Pauli and Ledergerber (Ref. 44) (open circles) and by Möller and Nix (Refs. 48 and 49) (solid circles). The lines show how A_H/A_L varies for a fixed A_H when A_f is varied.

potential-energy minima associated with two particular mass splits, (134+complement) and (142+complement) is plotted as a function of A_f as calculated by them. Their calculation predicts, in contradiction to our finding, that for $A_f \geq 238$ the mass split into the fragment mass 142 becomes more favored to the mass split into the fragment mass 134.

We would also like to point out that the constancy of the asymmetric peak positions of two Gaussians has been predicted by microscopic calculations of fission barriers. In Fig. 12 are plotted, as a function of A_f, heavy-to-light fragment mass ratios A_H/A_L predicted by Pauli and Ledergerber[44] and Möller and Nix[48,49] from the configuration of the nucleus at the fission barrier. The open circles are those predicted by Pauli and Ledergerber, who calculated the least-action trajectory and obtained A_H/A_L for the deforming nucleus at the dynamical fission barriers. They predict that the formation of $A_H=142$ is most favored for a wide range of A_f. The closed circles are those predicted by Möller and Nix, who calculated static fission barriers. They predict that if the static potential around the saddle point strongly influences the final mass division, the most probable mass split will be $A_H \sim 134$ for the fissioning nuclides $A_f \geq 238$, with A_H becoming smaller for $A_f \leq 236$. Therefore, the dynamical and the static saddle-point theory can explain either one of the two Gaussian peak positions but neither one of them alone can explain the two peak positions.

It should also be mentioned that during the final phase of the preparation of this paper, Hambsch *et al.*[50] published a paper on fission mode fluctuations in the resonance of $^{235}U(n,f)$ in which they made a similar two-Gaussian analysis of asymmetric mass yield peaks. They claim that the two Gaussians at $A \sim 133$ and $A \sim 147$ are produced by the two fission paths, standard I and standard II, predicted by Brosa *et al.*[42,43] and parametrized by Knitter *et al.*[51] Their results are generally in agreement with ours but more theoretical justification is needed to prove the presence of the two asymmetric fission paths after passing over the asymmetric barrier.

Finally, a word is given to the symmetric mass yield peak. A similar Gaussian analysis has been carried out to the symmetric peak (see Fig. 7), and it is found that three Gaussians are required, one centering around $A_f/2$ and the other around $A \sim 126$ and at its complementary mass.

CONCLUSION

Mass yield curves of proton-induced fissions of ^{232}Th, ^{233}U, ^{235}U, ^{238}U, ^{237}Np, ^{239}Pu, ^{242}Pu, ^{244}Pu, ^{241}Am, and ^{243}Am were studied. The correlation between the P/V ratio and the FWHM of the asymmetric mass yield peak was obtained as a function of proton energy. The FWHM values are rather independent of the incident proton energy as long as the P/V ratio is larger than 10 for all the fissioning systems studied. They become minimum in the region of the fissioning mass $A_f=240$–245, as previously reported for thermal-neutron–induced fissions and spontaneous fissions. A close examination of excitation functions of fission products reveals that there are at least two different threshold energies, one for the production of symmetric mass-split products and the other for the production of asymmetric products. With a simple assumption of the two-mode hypothesis, observed mass yield curves could be decomposed into two mass yield curves.

An attempt was also made to quantitatively understand the variation of the shapes of mass yield curves as a function of the mass of the fissioning nuclide. Asymmetric mass yield peaks could best be represented by the sum of two Gaussians, and their variation could be expressed by the variation of Gaussian parameters. The peak positions

of the two Gaussian are $A=133-135$ and $A=140-142$ for all the fissioning nuclides investigated. Preference of those fragment masses can partly be explained by both the scission-point model and the saddle-point model, but the variational trend of the relative heights of the two Gaussians is contrary to the prediction of the former model. More systematic data are needed for quantitative understanding of the variation of mass yield curves as a function of both Z and A of fissioning nuclides and for screening out improper models.

ACKNOWLEDGMENTS

The authors wish to thank the staff and crew of the Japan Atomic Energy Research Insitute (JAERI) tandem accelerator and the AVF cyclotron of Institute for Nuclear Study (INS). We would like to thank Dr. Y. Hatsukawa and Dr. T. Miura for helpful discussions, and Dr. S. Baba, Dr. T. Sekine, Dr. H. Kudo, and Dr. H. Umezawa at the Department of Radioisotopes of JAERI for helpful advice and support.

[1]M. Goeppet-Mayer, Phys. Rev. **74**, 235 (1948).
[2]P. Moller and S. G. Nilson, Phys. Lett. **31B**, 283 (1970).
[3]P. Moller, S. G. Nilsson, and J. R. Nix, Nucl. Phys. **A229**, 292 (1974).
[4]V. M. Strutinsky, Nucl. Phys. **A122**, 1 (1968).
[5]T. Ledergerber and H. C. Pauli, Nucl. Phys. **A207**, 1 (1973).
[6]B. D. Wilkins, E. P. Steinberg, and R. R. Chasman, Phys. Rev. C **14**, 1832 (1976).
[7]J. P. Unik, J. E. Gindler, L. E. Glendenin, K. F. Flynn, A. Gorski, and R. K. Sjoblom, *Physics and Chemistry of Fission 1973* (IAEA, Vienna, 1974), Vol. 11, p. 19.
[8]H. Thierens, A. De Clercq, E. Jacobs, D. De Frenne, P. D'hondt, P. De Gelder, and A. J. Deruytter, Phys. Rev. C **23**, 2104 (1981).
[9]E. Allaert, C. Wagemans, G. Wegener-Penning, A. J. Deruytter, and R. Barthélémy, Nucl. Phys. **A380**, 61 (1982).
[10]R. L. Ferguson, F. Plasil, F. Pleasonton, S. C. Burnett, and H. W. Schmitt, Phys. Rev. C **7**, 2510 (1973).
[11]J. N. Neiler, F. J. Walter, and H. W. Schmitt, Phys. Rev. **149**, 894 (1966).
[12]A. A. Naqvi, F. Käppeler, F. Dickmann, and R. Müller, Phys. Rev. C **34**, 218 (1986).
[13]T. Ohtsuki, Y. Nagame, Y. Hamajima, K. Sueki, and H. Nakahara (unpublished).
[14]Y. Hamajima, K. Sukei, T. Ohtsuki, H. Nakahara, and I. Kohno (unpublished).
[15]G. E. Gordon, J. W. Harvey, and H. Nakahra, Nucleonics **24**, 62 (1966).
[16]R. Collé, R. Kishore, and J. B. Cumming, Phys. Rev. C **9**, 1819 (1974).
[17]C. F. Williamson, J. P. Boujot, and J. Picard, Centre d'Etudes Nucleaires de Saclay Report CEA-R3042, 1966 (unpublished).
[18]L. C. Northcliffe and R. F. Schilling, Nucl. Data Sect. A **7**, 233 (1970).
[19]J. A. McHugh and M. C. Michel, Phys. Rev. **172**, 1160 (1968).
[20]H. R. Von Gunten, Actinides Rev. **1**, 275 (1969).
[21]K. F. Flynn, E. P. Horwits, C. A. A. Bloomquist, R. F. Barnes, R. K. Sjoblom, P. R. Fields, and L. E. Glendenin, Phys. Rev. C **5**, 1725 (1972).
[22]H. Thierens, E. Jacobs, P. D'hondt, A. De Clercq, M. Piessens, and D. De Frenne, Phys. Rev. C **29**, 498 (1984).
[23]M. G. Itkis, V. N. Okolovich, A. Ya. Rusanov, and G. N. Smirenkin, Yad. Fiz. **41**, 849 (1985) [Sov. J. Nucl. Phys. **41**, 544 (1985)].
[24]K. F. Flynn, J. E. Gindler, L. E. Glendenin, and R. K. Sjoblom, J. Inorg. Nucl. Chem. **38**, 661 (1976).
[25]H. Nakahara, T. Ohtsuki, Y. Hamajima, and K. Sueki, Radiochim. Acta **43**, 77 (1988).
[26]H. Nakahara, I. Fujiwara, H. Okamota, N. Imanishi, M. Ishibashi, T. Nishi, J. Inorg. Nucl. Chem. **33**, 3239 (1971).
[27]A. Ramaswami, S. P. Dange, S. Prakash, and M. V. Ramaniah, J. Inorg. Nucl. Chem. **41**, 1649 (1979).
[28]H. Kudo, H. Muramatsu, H. Nakahara, K. Miyano, and I. Kohno, Phys. Rev. C **25**, 3011 (1982).
[29]H. A. Tewes and R. A. James, Phys. Rev. **88**, 860 (1952).
[30]L. E. Glendenin, J. E. Gindler, I. Ahmad, D. J. Henderson, and J. W. Meadows, Phys. Rev. C **22**, 152 (1980).
[31]R. Eaker, H. S. Plendl, A. F. Zeller, A. Clem, L. Muga, and J. M. Nicovich, Phys. Rev. C **20**, 1055 (1979).
[32]C. F. Tsang and J. B. Wilhelmy, Nucl. Phys. **A184**, 417 (1972).
[33]H. Baba and S. Baba, Nucl. Phys. **A175**, 199 (1971).
[34]A. Turkevich and J. B. Niday, Phys. Rev. **84**, 52 (1951).
[35]H. C. Britt, H. E. Wegner, and J. C. Gursky, Phys. Rev. **129**, 2239 (1963).
[36]E. Konecny, H. J. Specht, and J. Weber, *Physics and Chemistry of Fission 1973* (IAEA, Vienna, 1974), Vol. II, p. 3.
[37]H. Kudo, Y. Nagame, H. Nakahara, K. Miyano, and I. Kohno Phys. Rev. C **25**, 909 (1982).
[38]D. G. Perry and A. W. Fairhall, Phys. Rev. C **4**, 977 (1971).
[39]A. Gayer and Z. Fraenkel, Phys. Rev. C **16**, 1066 (1977).
[40]S. Baba, H. Umezawa, and H. Baba, Nucl. Phys. **A175**, 177 (1971).
[41]V. V. Pashkevich, Nucl. Phys. **A169**, 275 (1971).
[42]U. Brosa, S. Grossman, and A. Müller, Z. Naturforsch. **41a**, 1341 (1986).
[43]U. Brosa and S. Grossmann, Z. Phys. A **310**, 177 (1983); S. Grossmann, U. Brossa, and A. Müller, Nucl. Phys. **A481**, 340 (1988).
[44]H. C. Pauli, T. Ledergerber, *Physics and Chemistry of Fission 1973* (IAEA, Vienna, 1974), Vol. I, p. 463.
[45]E. A. C. Crouch, Atomic Data Nucl. Data Tables **19**, 417 (1977).
[46]H. R. Von Gunten, K. F. Flynn, and L. E. Glendenin, Phys. Rev. **161**, 1192 (1967).
[47]Ch. Straede, C. Budtz-Jørgensen, and H.-H. Knitter, Nucl. Phys. **A462**, 85 (1987).
[48]P. Möller and J. R. Nix, Nucl. Phys. **A229**, 269 (1974).
[49]P. Möller, Nucl. Phys. **A192**, 529 (1972).
[50]F-J. Hambsch, H. H. Knitter, C. Budtz-Jørgensen, and J. P. Theobald, Nucl. Phys. **A491**, 56 (1989).
[51]H.-H. Knitter, F.-J. Hambsch, C. Budtz-Jørgensen, and J. P. Theobald, Z. Naturforsch **42a**, 786 (1987).